ACS APPLIED MATERIALS & INTERFACES

Research Article

www.acsami.org

Subnanometer Molybdenum Sulfide on Carbon Nanotubes as a Highly Active and Stable Electrocatalyst for Hydrogen Evolution Reaction

Ping Li,[†] Zhi Yang,*[,†] Juanxia Shen,[†] Huagui Nie,[†] Qiran Cai,[‡] Luhua Li,[‡] Mengzhan Ge,[†] Cancan Gu,[†] Xi'an Chen,[†] Keqin Yang,[†] Lijie Zhang,[†] Ying Chen,[‡] and Shaoming Huang*[,†]

[†]Nanomaterials & Chemistry Key Laboratory, Wenzhou University, Wenzhou 325027, China

[‡]ARC Centre of Excellence for Functional Nanomaterials, Institute for Frontier Materials, Deakin University, Waurn Ponds, Victoria 3216, Australia

Supporting Information

ABSTRACT: Electrochemically splitting water for hydrogen evolution reaction (HER) has been viewed as a promising approach to produce renewable and clean hydrogen energy. However, searching for cheap and efficient HER electrocatalysts to replace the currently used Pt-based catalysts remains an urgent task. Herein, we develop a one-step carbon nanotube (CNT) assisted synthesis strategy with CNTs' strong adsorbability to mediate the growth of subnanometer-sized MoS_x on CNTs. The subnanometer MoS_x-CNT hybrids achieve a low overpotential of 106 mV at 10 mA cm^{-2}, a small Tafel slope of 37 mV per decade, and an unprecedentedly high turnover frequency value of 18.84 s^{-1} at η = 200 mV among all reported non-Pt catalysts in acidic conditions. The superior performance of the hybrid catalysts benefits from the presence of a higher number of active sites and the abundant exposure of unsaturated S atoms rooted in the subnanometer structure, demonstrating a new class of subnanometer-scale catalysts.

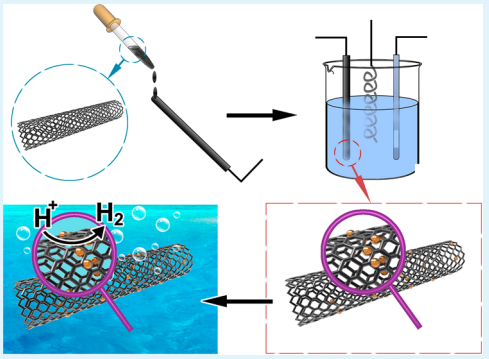

KEYWORDS: *subnanometer, molybdenum sulfide, carbon nanotubes, electrocatalysts, hydrogen evolution reaction*

INTRODUCTION

In recent years, rapidly increasing energy demands and the associated environmental issues have driven the development of renewable and clean energy sources.[1−3] Electrochemically splitting water via the hydrogen evolution reaction (HER), as a sustainable, secure, and environmentally benign energy vector, offers a promising solution for this purpose.[1] So far, the most effective electrocatalyst for HER is Pt or its alloys, but their high cost and limited supply hinder their large-scale practical applications.[2] Recently, various nanostructured molybdenum sulfides (MoS_x) prepared by different methods, such as chemical exfoliation,[3] chemical vapor deposition,[4,5] electrodeposition,[6] and solvothermal methods,[7,8] have received tremendous attention and become a promising alternative to Pt because of the potentially low cost and high catalytic activity of nanostructured MoS_x, which is due to a much higher specific surface area and more active sites compared with its bulk counterpart.[9−12] Despite significant success, nanometer-sized MoS_x-based HER electrocatalysts have not reached the same efficiency exhibited by Pt, and further improvement for their activity and stability remains an urgent task.

According to previous theories, there are three universal strategies to improve the HER activity of MoS_x-based catalysts: (1) increasing the number of active sites per unit volume; (2) enhancing the inherent activity of MoS_x; and (3) improving the conductivity and diffusion properties of the MoS_x materials.[13] Recent theoretical calculations and detailed experiments have shown that subnanometer-sized clusters have better catalytic activity than nanometer-sized particles in many catalytic fields because of the presence of more active sites together with the improved inherent activity rooted in the generation of new unsaturated active atoms after the catalysts are downsized.[14] In this sense, developing the MoS_x particles at a subnanometer scale as well as improving the conductivity of the whole catalyst system would seem to present an ideal solution to fully coordinate the three universal strategies detailed above and, thus, be highly desired to achieve high HER activity for MoS_x. However, to the best of our knowledge, studies involving the controllable preparation of subnanometer-sized MoS_x particles are still rare. The major reason for this may be due to the self-aggregation tendency of subnanometer-sized particles originating in their high surface energy. For instance, applying synthesis methods involving high temperature, such as chemical vapor deposition and solvothermal methods, to generate subnanometer-sized MoS_x particles seems to be very difficult because heat treatment can easily enlarge the size of particles.[13]

Received: September 17, 2015
Accepted: January 14, 2016
Published: January 14, 2016

DOI: 10.1021/acsami.5b08816
ACS Appl. Mater. Interfaces 2016, 8, 3543−3550

Table 1. Physical Parameters, Electrochemical Properties, and Corresponding Experimental Data for Various Carbon Materials

sample	deposition cycles	MoS_x content (wt %)	onset potential (mV)	Tafel slope (mV per dec)	current density at 10 mA cm^{-2} corresponding η (mV)	exchange current density (mA cm^{-2})
CNTs+20cyc[a]	20	0.75	90	44	143	8.1×10^{-3}
CNTs+30cyc[a]	30	0.98	48	37	106	1.4×10^{-2}
CNTs+40cyc[a]	40	1.21	100	47	171	5.2×10^{-3}
CNTs+100cyc[a]	100	2.01	162	59	235	8.0×10^{-4}
CNTs+30cyc[b]	30	5.52	180	64	242	6.3×10^{-4}
bare ele+30cyc[a]	30		200	54	302	1.6×10^{-4}

[a]2 mM $(NH_4)_2MoS_4$. [b]20 mM $(NH_4)_2MoS_4$.

Recently, Hu's groups developed a method to produce amorphous MoS_x materials on indium tin oxide (ITO) or fluorine-doped tin oxide (FTO) substrates via an electrodeposition process at room temperature. The amorphous MoS_x has many defect sites and coordinately unsaturated S atoms, which makes it a potentially better HER catalyst.[15] However, subnanometer-sized MoS_x particles still cannot be generated in all reported methods including electrodeposition methods.[16,17] Some previous studies have indicated that a strong interface interaction is necessary to anchor the formed small clusters (or single atoms) on the support and prevent their aggregation on the surface.[13,18] Therefore, it is believed that the relatively weak interaction between MoS_x and ITO (or FTO) substrates should be the main reason for the difficult formation of subnanometer-sized clusters. In this respect, searching for suitable support materials may be a key factor in the synthesis of subnanometer-sized MoS_x.

Herein, after comprehensively considering the inherent outstanding properties of carbon nanotubes (CNTs), such as high conductivity and strong adsorbability rooted in their surface energy,[19−23] we develop a one-step fabrication strategy via a simple electrodeposition procedure and achieve the in situ growth of subnanometer MoS_x clusters onto the CNTs. Spectroscopy characterizations such as X-ray photoelectron spectroscopy (XPS) and Raman spectroscopy confirm the existence of abundant unsaturated S atoms on the surface of the subnanometer particles and the well-coupled interface between MoS_x and CNTs. By virtue of the unique subnanometer structure, the as-prepared subnanometer MoS_x-CNTs hybrid catalysts (Sub-MoS_x-CNTs) achieve a low onset of 48 mV, a small Tafel slope of 37 mV per decade, and an excellent stability in acidic conditions for the HER. Furthermore, the Sub-MoS_x-CNTs have an unprecedentedly high turnover frequency (TOF) value for the HER among all previously reported nonprecious metal catalysts so far. The advisable use of the improved properties derived from the subnanometer-sized structure might offer vast new opportunities for applications in a variety of industrial chemical reactions.

EXPERIMENTAL SECTION

Electrode Preparation. Bare glassy carbon electrodes (GCE) (3 mm diameter, CH Instrument Inc.) were polished with a 0.05 and 0.3 μm alumina slurry on a microcloth and subsequently rinsed with ultrapure water and ethanol. The electrodes were then sonicated in ultrapure water, rinsed thoroughly with ultrapure water, and dried under a gentle nitrogen stream. To prepare the working electrode, a 2 mg CNT sample (CNTs were purchased from Cnano Technology (Beijing) Limited (http://www.cnanotechnology.com/en/pro.html, purity > 95%; diameter ~ 11 nm; length = 10 μm (average); synthesis method, CVD)) was ultrasonically dispersed in the mixed solution of ethanol and H_2O (500 mL), and then 8 μL of the resultant suspension was dropped onto the GCE surface and dried at room temperature. For comparison, a commercially available Pt/C-modified GCE (20 wt % Pt supported on carbon black, fuel cell grade from Alfa Aesar) was prepared in the same way.

Synthesis of Sub-MoS_x-CNTs. The hybrid catalysts were synthesized via a one-step electrochemical deposition method, wherein CNT-modified GCEs were soaked in a 2 mM $(NH_4)_2MoS_4$ aqueous solution containing 0.1 M $NaClO_4$, and the subnanometer MoS_x was deposited in situ onto CNTs by a potential cycling experiment at a scan rate of 50 mV s^{-1}. At the end of deposition, the working electrode was rinsed with water gently and dried under vacuum at room temperature overnight. All of the potentials in our paper are calibrated to a reversible hydrogen electrode (RHE) based on the Nernst equation. For comparison, bare GCEs without CNTs were treated under the same synthesis conditions, and parallel experiments using various deposition cycles and precursor concentrations were also carried out. The obtained hybrids were denoted CNTs+20cyc, CNTs +30cyc, CNTs+40cyc, and so on. Their physical parameters, electrochemical properties, and corresponding experimental data are listed in Table 1.

Structure Characterization. X-ray photoelectron spectroscopy (XPS) measurements were carried out with an ultrahigh-vacuum setup, equipped with a monochromatic Al KR X-ray source and a high-resolution Gammadata-Scienta SES 2002 analyzer. X-ray diffraction patterns (XRD) were obtained with a D/MAX-2400 diffractometer using Cu Kα radiation. Raman spectra were taken under ambient conditions using a Renishaw (inVia) with an Ar ion laser beam at an excitation wavelength of 532 (633) nm. SEM images were obtained with a JSM-6700 immersion scanning electron microscope. TEM analyses were carried out with a JEM-2100F instrument operating at 200 kV. Scanning transmission electron microscopy (STEM) characterizations were performed with an aberration-corrected Titan ChemiSTEM equipped with a probe corrector (CEOS).

Electrochemical Measurements. All electrochemical measurements, including cyclic voltammograms (CV) and linear sweep voltammograms (LSVs), were performed at room temperature in a three-electrode system at an electrochemical station (CH Instrument Inc.). A carbon catalyst electrode was used as working electrode, a Pt wire as counter electrode, and a SCE (3 M KCl filled) electrode as reference. LSV was recorded in 0.5 M H_2SO_4 solutions at a scan rate of 5 mV s^{-1} to obtain the polarization curves. The long-term stability tests were performed by continuous linear sweep voltammetry scans from −0.2 to −0.7 V (vs SCE, in 0.5 M H_2SO_4) at a scan rate of 50 mV s^{-1}. To estimate the double-layer capacitance, cyclic voltammograms taken with various scan rates (20, 40, 80, 160, 200 mV s^{-1}, etc.) were used under the potential window of 0−0.3 V versus RHE. Electrochemical impedance spectroscopy (EIS) was performed in the same configuration from 0.1 Hz to 10 kHz with an AC voltage of 5 mV. The polarization curves were replotted as overpotential (η) versus log current density (log j) to get Tafel plots for assessing the HER kinetics of investigated catalysts. By fitting the linear portion of the Tafel plots to the Tafel equation ($\eta = b \log (j) + a$), the Tafel slope (b) can be obtained. All data were reported without iR compensation. In all measurements, we used SCE as the reference electrode. It was calibrated with respect to RHE. The calibration was performed in the high-purity hydrogen-saturated electrolyte with a Pt foil as the working and counter electrodes. Cyclic voltammetry was run at a scan rate of 1 mV s^{-1}, and the average of the two potentials at which the current

DOI: 10.1021/acsami.5b08816
ACS Appl. Mater. Interfaces 2016, 8, 3543−3550

crossed 0 was taken to be the thermodynamic potential for the hydrogen electrode reaction. In 0.5 M H_2SO_4, E (RHE) = E (SCE) + 0.215 V. The detailed calculation of turnover frequency (TOF) is seen in the Supporting Information (Figure S16).

RESULTS AND DISCUSSION

Figure 1 schematically shows the entire synthesis procedure for the Sub-MoS_x-CNTs. Briefly, the hybrid catalysts were synthesized via a one-step electrochemical deposition method, wherein CNT-modified GCEs were soaked in $(NH_4)_2MoS_4$ aqueous solution containing $NaClO_4$, and the subnanometer MoS_x was in situ deposited onto the surface of the CNTs by a potential cycling experiment (Figure S1, see the Supporting Information). For comparison, bare GCEs without CNTs were also treated under the same synthesis conditions. Additionally, parallel experiments using various deposition cycles and precursor concentrations were carried out; the obtained hybrids were denoted CNTs+20cyc, CNTs+30cyc, CNTs+40cyc, and so on. Their physical parameters, electrochemical properties, and corresponding experimental data are listed in Table 1.

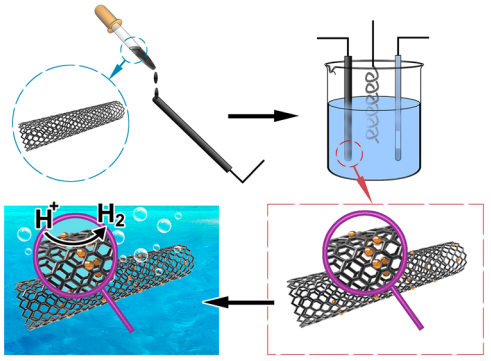

Figure 1. Schematic illustration of the synthesis procedure of Sub-MoS_x-CNTs.

Panels a–f of Figure 2 show typical scanning electron microscopy (SEM) and transmission electron microscopy (TEM) images for the CNTs+30cyc hybrid. Compared with that of pristine CNTs in Figure S2a,b, it can be found that abundant particles with a very small size have appeared and been highly dispersed on the surfaces of the CNTs. The enlarged SEM (Figure S3) and TEM images (Figures 2d,e and S4) confirm that most of these particles are at a subnanometer scale (white circled areas). The highlighted dots in the STEM and corresponding elemental mappings in Figures 2c and S5 display a uniform spatial distribution of subnanometer particles comprising Mo and S atoms on CNTs, which indicate the successful synthesis of subnanometer-sized MoS_x grown on CNTs. The heavy atoms in practical catalysts can be discerned in the aberration-corrected high-angle annular dark-field scanning transmission electron microscopy (HAADF-STEM). The HAADF-STEM and corresponding high-resolution transmission electron microscopy (HRTEM) images in Figure 2f,g show that the size of a typical subnanometer clusters is approximately 0.8 nm. Some unobvious lattices (white circled areas) appear in the region belonging to the subnanometer MoS_x particle, as shown in Figure 2f, which indicates that the formed MoS_x particle is amorphous. The XRD spectra for the CNTs+30cyc hybrid (Figure S6) show that no peaks of the corresponding MoS_x phase can be detected, which indicates a uniform distribution of the ultrasmall amorphous MoS_x in the hybrids.[24]

During the electrodeposition procedure by a potential cycling experiment, the electrodeposition cycles and the

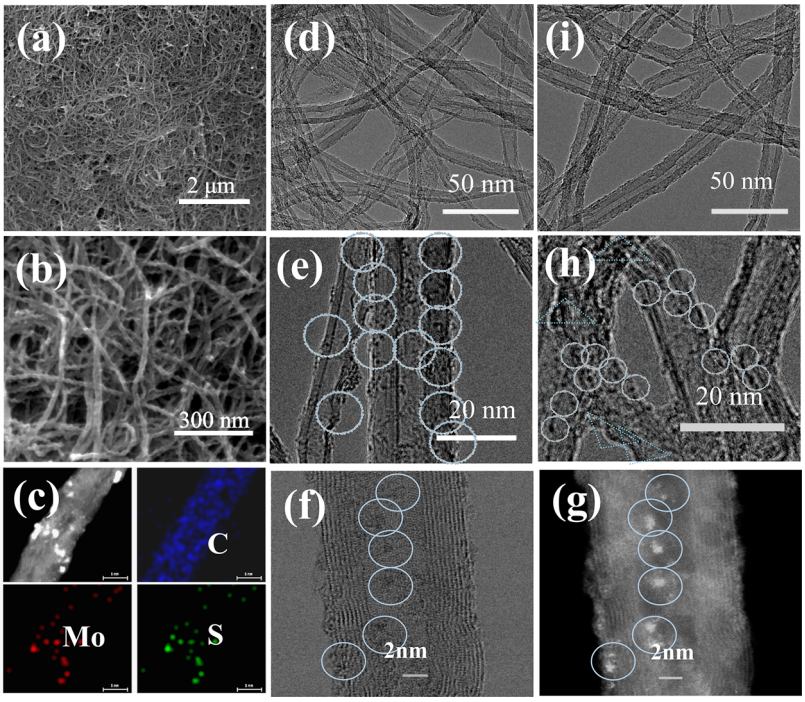

Figure 2. Characterization of the MoS_x-CNT hybrid catalysts: (a, b) SEM images of CNTs+30cyc hybrid; (c) STEM and corresponding element mapping of CNTs+30cyc hybrid (scale bar = 5 nm); (d, e) TEM images of CNTs+30cyc hybrid; (g, f) HAADF-STEM and corresponding HRTEM image of CNTs+30cyc hybrid; (h, i) TEM images of CNTs+40cyc hybrid. The circles and triangles in the images represent the subnanometer and aggregations, respectively.

DOI: 10.1021/acsami.5b08816
ACS Appl. Mater. Interfaces 2016, 8, 3543–3550

precursor concentrations are considered very important for determining the formation of the MoS_x-CNTs hybrids. As expected, the loading of MoS_x on CNTs increases with increasing deposition cycle or precursor concentration. The measurements for inductively coupled plasma-atom emission spectroscopy and elemental analysis also confirm this hypothesis, as the loading values for the samples obtained using deposition cycles of 20, 30, 40, and 100 are 0.75, 0.98, 1.21, and 2.01 wt %, respectively (Table 1). Furthermore, from the SEM and TEM images for MoS_x-CNTs hybrids obtained at various deposition cycles in Figures 2h,i and S2, S7, S8, and S9, it can be seen that the subnanometer-sized particles have commenced aggregation and some larger particles or films at the nanometer scale (white triangular areas) are formed when the number of deposition cycles is beyond 40. The TEM images in Figure 3 also show that the subnanometer-sized

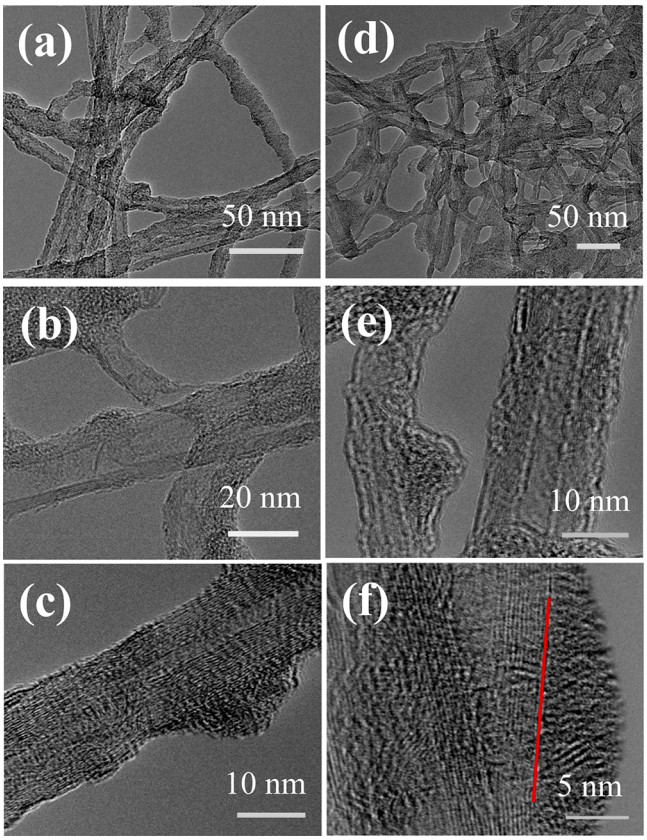

Figure 3. TEM images of the MoS_x-CNTs hybrids obtained at high precursor concentrations: (a–c) 20 mM $(NH_4)_2MoS_4$; (d–f) 50 mM $(NH_4)_2MoS_4$.

particles almost disappear and larger particles at the nanometer scale are present when the precursor concentration is increased to 20 and 50 mM. These morphological characterizations also suggest that a relatively short deposition time and low precursor concentration should be beneficial for forming subnanometer-sized MoS_x particles. To further understand the formation mechanism for the subnanometer-sized MoS_x, we compare previous studies involving MoS_x fabrication via electrodeposition. Although several investigations involving MoS_x fabrication on nanocarbon substrates via an electrodeposition method have been reported,[15,16,25] to our knowledge, MoS_x particles of the size <1 nm have not been reported previously. After comparatively analyzing the detailed experimental information in Table S1, it is found that the quantity of electrodeposited sediment in our experiments can be more accurately controlled because of our shorter deposition time or lower supporting electrolyte concentration compared with those of previous studies. These results also indicate that the more accurately controlled experiment under a slower reaction rate and shorter reaction time should play a vital role in determining the formation of subnanometer-sized particles.

The elemental composition and bonding configuration of the CNTs+30cyc were investigated using XPS. The survey spectrum in Figure 4a shows the predominant signals of carbon, molybdenum, and sulfur. The states of sulfur and molybdenum species in the sample are determined from the high-resolution XPS S 2p and Mo 3d spectra. In Figure 4b, the deconvolution of the Mo 3d region by peak fitting reveals that the doublet with a $3d_{5/2}$ binding energies of 229.4 eV is attributed to Mo(IV), and another doublet at 233 eV is due to the Mo(VI) ion, which might come from oxidation of the particles during deposition or during the sample transfer process for XPS measurement.[10,25,26] The S 2p spectrum in Figure 4c shows a broad and complex peak with three distinct doublets. The S $2p_{3/2}$ at 162.0 eV can be attributed to terminal S_2^{2-} ligands, and the S $2p_{3/2}$ at 163.6 eV represents bridging S_2^{2-} and/or apical S^{2-} ligands.[2,25,27] The S $2p_{3/2}$ doublet at higher energy (164.3 eV) can be attributed to residual sulfur from the electrodeposition reactant.[2] Furthermore, the ratio of S to Mo is calculated to be approximately 3.6, which is larger than commonly reported for MoS_x ($x \approx 3$). This is also a strong indication for the presence of abundant unsaturated S active edges on the surface of the Sub-MoS_x-CNTs.[9,28] Some recent papers have proposed that the abundant exposure of the terminal S_2^{2-} and bridging S_2^{2-} ligands in amorphous MoS_x can effectively absorb H with a small free energy, which is advantageous for the great enhancement of the HER activity.[10,11,29] Therefore, it is believed that CNTs+30cyc with abundant active S edge sites should give potentially outstanding HER performance. Raman characterization is also in good agreement with the XPS results. The vibration at 540 cm^{-1} belongs to the S–S vibrations of the terminal S_2^{2-} and bridging S_2^{2-} ligands in addition to other bands at 230 cm^{-1} as shown in Figure 4d, and the peaks at 350 and 470 cm^{-1} correspond to Mo–S vibrations from the sample.[9,30,31]

To examine the state of the coupled interface between MoS_x and CNTs, the CNTs+30cyc sample was ultrasonically dispersed in H_2O. The XPS results showed no change in the levels of S and Mo before and after sonication, which suggests the existence of strong coupled interactions between MoS_x and CNTs. Furthermore, the states of C species occurring in CNTs +30cyc and pristine CNTs were further compared using the high-resolution XPS C 1s spectrum. The high-resolution C 1s spectrum of CNTs+30cyc shows a broader signal, compared with that of pristine CNTs (Figure S10).[32] This further supports the above-mentioned result involving the existence of well-coupled interactions. On the basis of Zhang's report, a strongly coupled interaction should play a vital role in stabilizing the formed subnanometer-sized species and preventing their aggregation on the surface.[14] Therefore, herein, it can be concluded that CNTs' strong adsorbability rooted in their surface energy should be an essential factor for achieving the successful synthesis of subnanometer-sized particles. This CNT-assisted synthesis strategy has not been proposed in any previous papers.

DOI: 10.1021/acsami.5b08816
ACS Appl. Mater. Interfaces 2016, 8, 3543–3550

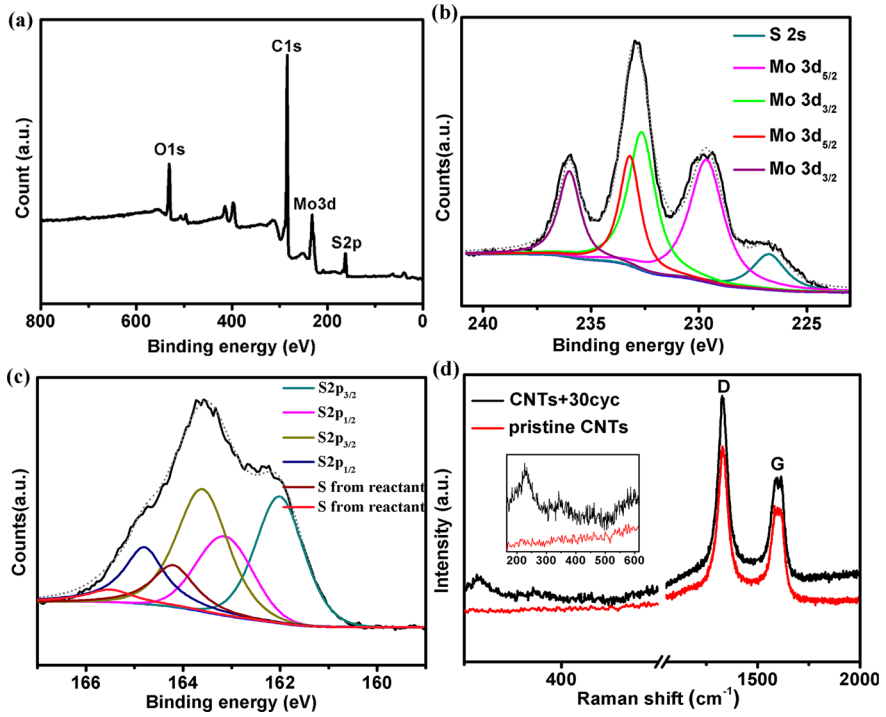

Figure 4. Characterizations of the CNTs+30cyc hybrid: (a) survey spectrum; (b) Mo 3d spectrum; (c) S 2p spectrum; (d) Raman spectra of CNTs +30cyc and pristine CNTs.

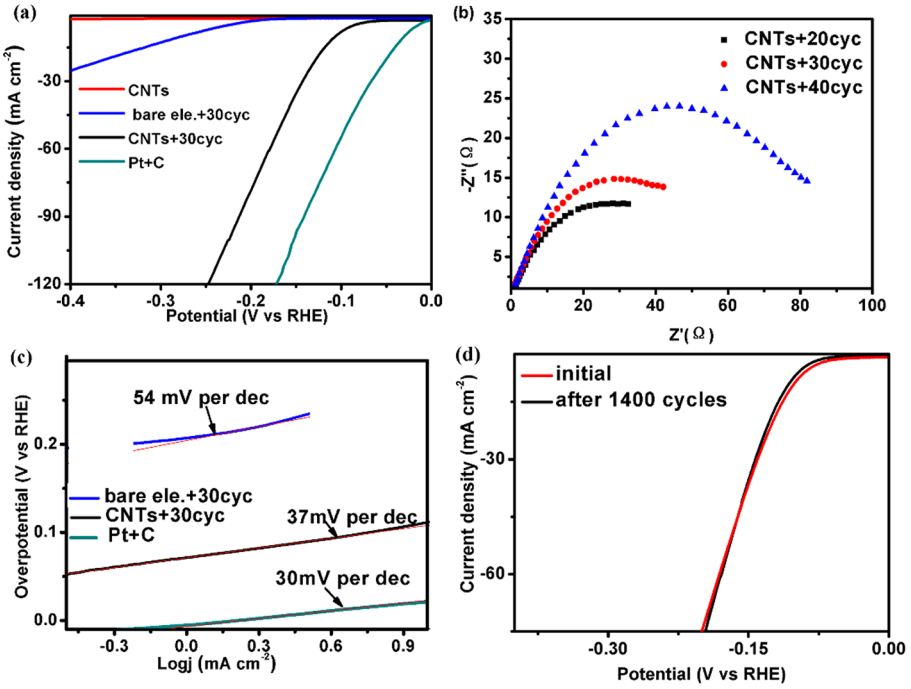

Figure 5. Electrochemical characterizations of the MoS_x-CNTs hybrid catalysts: (a) polarization curves at 5 mV s^{-1} in 0.5 M H_2SO_4; (b) Nyquist plots of MoS_x-CNTs hybrid catalysts; (c) Tafel plots of the hybrid with different deposition cycles; (d) long-term cycling test for the CNTs+30cyc at 50 mV s^{-1}.

The HER activities of various Sub-MoS_x-CNTs catalysts were evaluated under acidic conditions (0.5 M H_2SO_4) in a typical three-electrode configuration to compare with pristine CNTs, commercial Pt/C, and bare ele+30cyc catalysts, as illustrated in Figure 5a. Their physical parameters, electrochemical properties, and corresponding experimental data are listed in Table 1. As a typical reference metric for electrochemical catalytic performance, the CNTs+30cyc catalyst shows a high activity for the HER, with an onset potential of 48 mV[1] (Figure S11) and a 106 mV overpotential necessary to achieve a 10 mA cm^{-2}, which is comparable to or better than any molybdenum sulfide-based HER catalyst reported to date (see Table S2). For the bare ele+30cyc electrode, a very negative onset potential of 200 mV and a low catalytic current

DOI: 10.1021/acsami.5b08816
ACS Appl. Mater. Interfaces 2016, 8, 3543−3550

can be observed, which indicates inferior HER performance, whereas the pristine CNT electrode exhibits only a small amount of HER activity. After combining CNTs and MoS_x, all of the Sub-MoS_x-CNTs catalysts show more positive onset potential and higher catalytic current than that of bare ele +30cyc or pristine CNTs electrodes (Figure S12). These experimental results indicate that the strategy involving hybridization of MoS_x with CNTs was highly effective for enhancing the HER activity because the presence of CNTs leads to rapid electron transport. Furthermore, from Figures 5a and S12, it can also be seen that CNTs+30cyc has the most positive onset potential and the highest catalytic current of all of the Sub-MoS_x-CNT samples, and increasing or decreasing the deposition cycles leads to a decrease in the activity of these MoS_x-CNTs hybrid catalysts. The varying activity of these counterparts might be a result of their various loading and surface morphology differences. To further investigate the effect of active surface area of the catalyst on the HER activity, we performed the EIS analysis of the Sub-MoS_x-CNT composites with various deposition cycles. The obtained Nyquist plot is shown in Figure 5b, and their electrical equivalent circuit diagram shown in Figure S13 was used to model the solid−liquid interface after the experimental data were well fitted. The impedance parameters by fitting the EIS responses are listed in Table S3. It is noted from Table S3 that CNTs+30cyc have a low R_p value of 59.4 Ω, and the largest CPE value among all of the composite catalysts. The low R_p value indicated its faster surface charge transfer and higher reaction rate in the electrocatalysis kinetics. The large CPE value corresponds to its high active surface area, which can strongly promote the HER performance. These may be the main reason that CNTs +30cyc have the highest HER activity among all of the composite catalysts. In other words, the Sub-MoS_x-CNTs composites with fewer deposition cycles (fewer than 30 cycles) should be short of the active sites, whereas the longer cycles (beyond 40 cycles) could lead to the formation of MoS_x agglomerations with larger size (Figure S8), thus decreasing the density of the edge activity sites and increasing the charge transfer resistance (Table S3).

To understand the detailed mechanism of HER activity of the subnanometer-sized catalysts, the Tafel slopes, based on polarization curves, are acquired and presented in Figures 5c and S14. A Tafel slope of 37 mV per decade was measured for CNTs+30cyc, similar to the value of 30 mV per decade for the Pt/C catalyst and lower than that of 54 mV per decade for bare ele+30cyc. The observed Tafel slope of 37 mV per decade suggests that the electrochemical desorption of hydrogen is the rate-limiting step in the HER for CNTs+30cyc.[33,34] To the best of our knowledge, this Tafel slope of 37 mV per decade is also comparable to or lower than that of all the reported noble-metal-free HER catalysts in the literature (Table S2). By applying the extrapolation method to the Tafel plot, the exchange current densities (j_0) were obtained, as shown in Tables S2 and S4 and Figure S15. The CNTs+30cyc electrode exhibits a remarkable exchange current density of 0.014 mA cm^{-2}, which is almost 90 times larger than the value of bare ele +30cyc and better than that of most non-Pt catalysts (Table S2), suggesting the excellent activity of CNTs+30cyc for HER catalysis.

The electrochemical method was used to estimate the activity of each catalytic site, an important metric necessary to appraise catalyst materials and to guide catalyst development, to engender the TOF of the catalyst. Because the subnanometer-sized MoS_x in our case has almost entire exposure of the active sites on its surface, rather than only a small amount of exposure for the bulk materials, presenting TOF value based on weight ratio of CNTs and Mo along with TOF per site should be a suitable method (detailed calculations are given on p S-20 of the Supporting Information). The calculation of TOF value based on weight ratio of CNTs and Mo along with TOF per site, the number of surface active sites of CNTs+30cyc is estimated to be 1.3×10^{16} cm^{-2}, and the corresponding TOF is 18.84 s^{-1} at η = 200 mV, which is about 4 times higher than that of the best reported nonprecious metal catalyst (Table S2). Also, according to Jaramillo's method (detailed calculations are given in Figure S16), the number of surface active sites of CNTs+30cyc is estimated to be 2.0×10^{16} cm^{-2}, and the corresponding TOF is as high as 12.25 s^{-1} at η = 200 mV versus RHE and TOF = 2.2×10^{-3} s^{-1} at η = 0 V versus RHE, which is close to the result calculated by weight ratio of CNTs and Mo described above. (TOF at zero overpotential is a measure of intrinsic catalytic activity, representing a chemical reaction rate. It is the metric to guide catalyst development.)[13,35] To better understand the origin of this high TOF value, the samples obtained under different deposition cycles are compared in Table 2; it can be seen that the CNTs+30cyc has the most surface active sites among all of these MoS_x-CNTs hybrids obtained at various deposition cycles, despite its lower MoS_x loading compared to CNTs+40cyc. This further confirmed the conclusion that downsizing the catalysts to subnanometer scale can generate more active sites. Furthermore, it is also found that the CNTs+40cyc, which comprises larger MoS_x particles at the nanometer scale, has an obviously lower TOF value than CNTs+20cyc and CNTs+30cyc. After referencing their different morphological and structural characterizations, it is believed that the exposure of coordinately unsaturated S atoms with high activation rooted in the subnanometer structure should be one of the most important factors affecting the high TOF value.[36] Additionally, on the basis of the electrochemical impedance spectroscopy analysis in Figure 5b, it is inferred that the highly effective electron transfer due to the use of CNTs may be another important factor for the high TOF value.

Table 2. Turnover Frequency (TOF) of the MoS_x-CNT Hybrid Catalysts

sample	TOF[a] (s^{-1})	TOF[b] (s^{-1})
CNTs+20cyc	11.84	1.8×10^{-3}
CNTs+30cyc	12.25	2.2×10^{-3}
	18.84[c]	
CNTs+40cyc	3.02	1.0×10^{-3}
bare ele+30cyc	0.9	3.0×10^{-4}

[a]TOFs were measured at η = 200 mV vs RHE. [b]TOFs were measured at η = 0 V vs RHE. [c]TOFs were measured by the weight ratio of CNTs and Mo.

The long-term cycling stability of CNTs+30cyc was assessed by performing continuous linear sweep voltammetry at 50 mV s^{-1}. The polarization curve of the CNTs+30cyc catalyst after 1400 cycles overlays almost exactly with the initial one (Figure 5d), with negligible loss of cathodic current, suggesting the catalyst is highly stable and can withstand accelerated degradation. This high durability is much higher than most previously reported MoS_x-carbon hybrid catalysts.[11] The superior durability of MoS_x-CNTs hybrid catalysts may be

DOI: 10.1021/acsami.5b08816
ACS Appl. Mater. Interfaces 2016, 8, 3543−3550

related to the strong coupling interaction between MoS_x and the CNT support. The exceptional long-term durability as well as the superior HER activity described above makes the CNTs +30cyc a promising HER catalyst for practical applications.

In this work, a one-step fabrication strategy via an electrodeposition method using the strong adsorbability of CNTs is examined; this technique is facile and easily reproducible to synthesize subnanometer-sized MoS_x particles onto CNTs. Compared with Hu's synthesis methods on ITO (or FTO) substrates, the CNTs, a support material with negligible HER activity by itself, can not only couple well with MoS_x to accelerate electron transfer and promote the HER activity but may also serve as an effective support to mediate the growth morphology of MoS_x to form subnanometer structures. Benefiting from the subnanometer structure, the as-prepared Sub-MoS_x-CNTs exhibit excellent electrocatalytic activity for HER. In particular, the TOF value of the Sub-MoS_x-CNTs for HER achieves an unprecedented height among all reported nonprecious metal catalysts. Considering the unique morphological and structural characterizations for the Sub-MoS_x-CNTs, it is inferred that the improved mechanism for the high HER performance might be attributed to the following aspects. (1) The subnanometer-sized MoS_x in the hybrids possesses exceptional intrinsic HER activity because of the abundant exposure of the terminal S_2^{2-} and bridging S_2^{2-} ligands on its surface. The unsaturated S atoms can effectively absorb H with a small free energy and promote the HER activity.[10,11,29] (2) The subnanometer size of the hybrid catalysts can provide more active sites for HER than larger-sized catalysts. (3) After comprehensively considering the inherent properties of CNTs as supporting materials, it is expected that the hollow tube-like structure of CNTs, as well as the well-coupled interface between MoS_x and CNTs is favorable to facilitate the charge and reactant transport, thus promoting the hydrogen production process. Of course, more in-depth investigations are needed to reveal the detailed mechanism derived from the novel subnanometer MoS_x structure.

CONCLUSION

In summary, we have achieved the successful fabrication of subnanometer-sized MoS_x particles grown on CNTs, using a CNT-assisted synthesis strategy with CNTs' strong adsorbability to mediate the growth of subnanometer-sized MoS_x. This Sub-MoS_x-CNT catalyst shows an onset potential of approximately 48 mV, a small Tafel slope of 37 mV per decade, a high exchange current density of 0.014 mA cm^{-2}, and a TOF of 12.25 s^{-1} (18.84 s^{-1} based on the weight ratio of CNTs and Mo) at η = 200 mV versus RHE. We attribute this high activity to the fact that the subnanometer structure can provide more active sites and expose more unsaturated S atoms, leading to highly efficient charge and reactant transport. The facile nature, versatility, and scalability of this method mean that it has great potential for the preparation of other subnanometer-sized catalyst-decorated carbon materials for constructing highly efficient HER electrocatalysts or more subnanometer structures for other catalytic, electronic, and optical applications.

ASSOCIATED CONTENT

Supporting Information

The Supporting Information is available free of charge on the ACS Publications website at DOI: 10.1021/acsami.5b08816.

Images of supplementary electrodeposition; morphological and structural characteristic performance; calculation of TOF of the material (PDF)

AUTHOR INFORMATION

Corresponding Authors

*(Z.Y.) E-mail: yang201079@126.com.

*(S.H.) E-mail: smhuang@wzu.edu.cn.

Notes

The authors declare no competing financial interest.

ACKNOWLEDGMENTS

The work was supported in part by grants from NSFC (21273163, 51572197, 21475096, and 51420105002), NSFZJ (LY13B050002), and Zhejiang Science and Technology Project (2014C31155). We acknowledge Prof. Chuanhong Jin and Zhangru Xiao of Zhejiang University for assistance in the aberration-corrected electron microscopy characterization. The work made use of the resources of the Center of Electron Microscopy of Zhejiang University.

REFERENCES

(1) Wu, H. B.; Xia, B. Y.; Yu, L.; Yu, X. Y.; Lou, X. W. D. Porous Molybdenum Carbide Nano-Octahedrons Synthesized via Confined Carburization in Metal-Organic Frameworks for Efficient Hydrogen Production. *Nat. Commun.* **2015**, *6*, 6512.

(2) Kibsgaard, J.; Jaramillo, T. F.; Besenbacher, F. Building an Appropriate Active-Site Motif into a Hydrogen-Evolution Catalyst with Thiomolybdate $[Mo_3S_{13}]^{2-}$ Clusters. *Nat. Chem.* **2014**, *6*, 248–253.

(3) Lukowski, M. A.; Daniel, A. S.; Meng, F.; Forticaux, A.; Li, L.; Jin, S. Enhanced Hydrogen Evolution Catalysis from Chemically Exfoliated Metallic MoS_2 Nanosheets. *J. Am. Chem. Soc.* **2013**, *135*, 10274–10277.

(4) Ji, Q.; Zhang, Y.; Zhang, Y.; Liu, Z. Chemical Vapour Deposition of Group-VIB Metal Dichalcogenide Monolayers: Engineered Substrates from Amorphous to Single Crystalline. *Chem. Soc. Rev.* **2015**, *44*, 2587–2602.

(5) Yu, Y.; Huang, S. Y.; Li, Y.; Steinmann, S. N.; Yang, W.; Cao, L. Layer-Dependent Electrocatalysis of MoS_2 for Hydrogen Evolution. *Nano Lett.* **2014**, *14*, 553–558.

(6) Murugesan, S.; Akkineni, A.; Chou, B. P.; Glaz, M. S.; Vanden Bout, D. A.; Stevenson, K. J. Room Temperature Electrodeposition of Molybdenum Sulfide for Catalytic and Photoluminescence Applications. *ACS Nano* **2013**, *7*, 8199–8205.

(7) Lu, Z.; Zhu, W.; Yu, X.; Zhang, H.; Li, Y.; Sun, X.; Wang, X.; Wang, H.; Wang, J.; Luo, J.; Lei, X.; Jiang, L. Ultrahigh Hydrogen Evolution Performance of Under-Water "Superaerophobic" MoS_2 Nanostructured Electrodes. *Adv. Mater.* **2014**, *26*, 2683–2687.

(8) Zhao, Y.; Zhao, F.; Wang, X.; Xu, C.; Zhang, Z.; Shi, G.; Qu, L. Graphitic Carbon Nitride Nanoribbons: Graphene-Assisted Formation and Synergic Function for Highly Efficient Hydrogen Evolution. *Angew. Chem., Int. Ed.* **2014**, *53*, 13934–13939.

(9) Wang, T.; Zhuo, J.; Du, K.; Chen, B.; Zhu, Z.; Shao, Y.; Li, M. Electrochemically Fabricated Polypyrrole and MoSx Copolymer Films as a Highly Active Hydrogen Evolution Electrocatalyst. *Adv. Mater.* **2014**, *26*, 3761–3766.

(10) Benck, J. D.; Chen, Z.; Kuritzky, L. Y.; Forman, A. J.; Jaramillo, T. F. Amorphous Molybdenum Sulfide Catalysts for Electrochemical Hydrogen Production: Insights into the Origin of their Catalytic Activity. *ACS Catal.* **2012**, *2*, 1916–1923.

(11) Li, D. J.; Maiti, U. N.; Lim, J.; Choi, D. S.; Lee, W. J.; Oh, Y.; Lee, G. Y.; Kim, S. O. Molybdenum Sulfide/N-Doped CNT Forest Hybrid Catalysts for High-Performance Hydrogen Evolution Reaction. *Nano Lett.* **2014**, *14*, 1228–1233.

(12) Gao, M. R.; Liang, J. X.; Zheng, Y. R.; Xu, Y. F.; Jiang, J.; Gao, Q.; Li, J.; Yu, S. H. An Efficient Molybdenum Disulfide/Cobalt Diselenide Hybrid Catalyst for Electrochemical Hydrogen Generation. *Nat. Commun.* **2015**, *6*, 5982.
(13) Yan, Y.; Xia, B.; Xu, Z.; Wang, X. Recent Development of Molybdenum Sulfides as Advanced Electrocatalysts for Hydrogen Evolution Reaction. *ACS Catal.* **2014**, *4*, 1693−1705.
(14) Yang, X. F.; Wang, A.; Qiao, B.; Li, J.; Liu, J.; Zhang, T. Single-Atom Catalysts: A New Frontier in Heterogeneous Catalysis. *Acc. Chem. Res.* **2013**, *46*, 1740−1748.
(15) Merki, D.; Fierro, S.; Vrubel, H.; Hu, X. Amorphous Molybdenum Sulfide Films as Catalysts for Electrochemical Hydrogen Production in Water. *Chem. Sci.* **2011**, *2*, 1262−1267.
(16) Laursen, A. B.; Vesborg, P. C.; Chorkendorff, I. A High-Porosity Carbon Molybdenum Sulphide Composite with Enhanced Electrochemical Hydrogen Evolution and Stability. *Chem. Commun.* **2013**, *49*, 4965−4967.
(17) Pu, Z.; Liu, Q.; Asiri, A. M.; Obaid, A. Y.; Sun, X. Graphene Film-Confined Molybdenum Sulfide Nanoparticles: Facile One-Step Electrodeposition Preparation and Application as a Highly Active Hydrogen Evolution Reaction Electrocatalyst. *J. Power Sources* **2014**, *263*, 181−185.
(18) Tian, J.; Liu, Q.; Asiri, A. M.; Sun, X. Self-Supported Nanoporous Cobalt Phosphide Nanowire Arrays: An Efficient 3D Hydrogen-Evolving Cathode over the Wide Range of pH 0−14. *J. Am. Chem. Soc.* **2014**, *136*, 7587−7590.
(19) Li, J.; Ke, C. T.; Liu, K.; Li, P.; Liang, S.; Finkelstein, G.; Wang, F.; Liu, J. Importance of Diameter Control on Selective Synthesis of Semiconducting Single-walled Carbon Nanotubes. *ACS Nano* **2014**, *8*, 8564−8572.
(20) Lee, W. J.; Maiti, U. N.; Lee, J. M.; Lim, J.; Han, T. H.; Kim, S. O. Nitrogen-Doped Carbon Nanotubes and Graphene Composite Structures for Energy and Catalytic Applications. *Chem. Commun.* **2014**, *50*, 6818−6830.
(21) Maiti, U. N.; Lee, W. J.; Lee, J. M.; Oh, Y.; Kim, J. Y.; Kim, J. E.; Shim, J.; Han, T. H.; Kim, S. O. 25th Anniversary Article: Chemically Modified/Doped Carbon Nanotubes & Graphene for Optimized Nanostructures & Nanodevices. *Adv. Mater.* **2014**, *26*, 40−67.
(22) Li, C.; Shi, G. Functional Gels Based on Chemically Modified Graphenes. *Adv. Mater.* **2014**, *26*, 3992−4012.
(23) Lee, W. J.; Choi, D. S.; Lee, S. H.; Lim, J.; Kim, J. E.; Li, D. J.; Lee, G. Y.; Kim, S. O. Electroless Bimetal Decoration on N-Doped Carbon Nanotubes and Graphene for Oxygen Reduction Reaction Catalysts. *Part. Part. Syst. Charact.* **2014**, *31*, 965−970.
(24) Song, J.; Gordin, M. L.; Xu, T.; Chen, S.; Yu, Z.; Sohn, H.; Lu, J.; Ren, Y.; Duan, Y.; Wang, D. Strong Lithium Polysulfide Chemisorption on Electroactive Sites of Nitrogen-Doped Carbon Composites for High-Performance Lithium−Sulfur Battery Cathodes. *Angew. Chem.* **2015**, *127*, 4399−4403.
(25) Vrubel, H.; Hu, X. Growth and Activation of an Amorphous Molybdenum Sulfide Hydrogen Evolving Catalyst. *ACS Catal.* **2013**, *3*, 2002−2011.
(26) Li, Y.; Yu, Y.; Huang, Y.; Nielsen, R. A.; Goddard, W. A., III; Li, Y.; Cao, L. Engineering the Composition and Crystallinity of Molybdenum Sulfide for High-Performance Electrocatalytic Hydrogen Evolution. *ACS Catal.* **2015**, *5*, 448−455.
(27) Wang, H. W.; Skeldon, P.; Thompson, G. E. XPS Studies of MoS_2 Formation from Ammonium Tetrathiomolybdate Solutions. *Surf. Coat. Technol.* **1997**, *91*, 200−207.
(28) Ge, X.; Chen, L.; Zhang, L.; Wen, Y.; Hirata, A.; Chen, M. Nanoporous Metal Enhanced Catalytic Activities of Amorphous Molybdenum Sulfide for High-Efficiency Hydrogen Production. *Adv. Mater.* **2014**, *26*, 3100−3104.
(29) Zheng, Y.; Jiao, Y.; Jaroniec, M.; Qiao, S. Z. Advancing the Electrochemistry of the Hydrogen-Evolution Reaction through Combining Experiment and Theory. *Angew. Chem., Int. Ed.* **2015**, *54*, 52−65.
(30) Weber, T.; Muijsers, J. C.; Niemantsverdriet, J. W. Structure of Amorphous MoS_3. *J. Phys. Chem.* **1995**, *99*, 9194−9200.
(31) Fedin, V. P.; Kolesov, B. A.; Mironov, Y. V.; Fedorov, V. Y. Synthesis and Vibrational (IR and Raman) Spectroscopic Study of Triangular Thio-Complexes $[Mo_3S_{13}]^{2-}$ Containing ^{92}Mo, ^{100}Mo and ^{34}S Isotopes. *Polyhedron* **1989**, *8*, 2419−2423.
(32) Yang, Z.; Yao, Z.; Li, G.; Fang, G.; Nie, H.; Liu, Z.; Zhou, X.; Chen, X.; Huang, S. Sulfur-Doped Graphene as an Efficient Metal-Free Cathode Catalyst for Oxygen Reduction. *ACS Nano* **2012**, *6*, 205−211.
(33) Gong, M.; Zhou, W.; Tsai, M. C.; Zhou, J.; Guan, M.; Lin, M. C.; Zhang, B.; Hu, Y.; Wang, D. Y.; Yang, J.; Pennycook, S. J.; Hwang, B. J.; Dai, H. Nanoscale Nickel Oxide/Nickel Heterostructures for Active Hydrogen Evolution Electrocatalysis. *Nat. Commun.* **2014**, *5*, 4695.
(34) Pan, Y.; Liu, Y.; Zhao, J.; Yang, K.; Liang, J.; Liu, D.; Hu, W.; Liu, D.; Liu, Y.; Liu, C. Monodispersed Nickel Phosphide Nanocrystals with Different Phases: Synthesis, Characterization and Electrocatalytic Properties for Hydrogen Evolution. *J. Mater. Chem. A* **2015**, *3*, 1656−1665.
(35) Costentin, C.; Drouet, S.; Robert, M.; Savéant, J. M. A Local Proton Source Enhances CO_2 Electroreduction to CO by a Molecular Fe Catalyst. *Science* **2012**, *338*, 90−94.
(36) Benck, J. D.; Hellstern, T. R.; Kibsgaard, J.; Chakthranont, P.; Jaramillo, T. F. Catalyzing the Hydrogen Evolution Reaction (HER) with Molybdenum Sulfide Nanomaterials. *ACS Catal.* **2014**, *4*, 3957−3971.

DOI: 10.1021/acsami.5b08816
ACS Appl. Mater. Interfaces 2016, 8, 3543−3550